TC271
Characterization Report

Jeffrey S. Campbell
Image Sensor Technology Center
Texas Instruments Incorporated
Dallas, Texas

SEPTEMBER 1994
SOCA004

TEXAS INSTRUMENTS

IMPORTANT NOTICE

Texas Instruments (TI) reserves the right to make changes to its products or to discontinue any semiconductor product or service without notice, and advises its customers to obtain the latest version of relevant information to verify, before placing orders, that the information being relied on is current.

TI warrants performance of its semiconductor products and related software to the specifications applicable at the time of sale in accordance with TI's standard warranty. Testing and other quality control techniques are utilized to the extent TI deems necessary to support this warranty. Specific testing of all parameters of each device is not necessarily performed, except those mandated by government requirements.

Certain applications using semiconductor products may involve potential risks of death, personal injury, or severe property or environmental damage ("Critical Applications").

TI SEMICONDUCTOR PRODUCTS ARE NOT DESIGNED, INTENDED, AUTHORIZED, OR WARRANTED TO BE SUITABLE FOR USE IN LIFE-SUPPORT APPLICATIONS, DEVICES OR SYSTEMS OR OTHER CRITICAL APPLICATIONS.

Inclusion of TI products in such applications is understood to be fully at the risk of the customer. Use of TI products in such applications requires the written approval of an appropriate TI officer. Questions concerning potential risk applications should be directed to TI through a local SC sales office.

In order to minimize risks associated with the customer's applications, adequate design and operating safeguards should be provided by the customer to minimize inherent or procedural hazards.

TI assumes no liability for applications assistance, customer product design, software performance, or infringement of patents or services described herein. Nor does TI warrant or represent that any license, either express or implied, is granted under any patent right, copyright, mask work right, or other intellectual property right of TI covering or relating to any combination, machine, or process in which such semiconductor products or services might be or are used.

Introduction

The purpose of this document is to summarize the characterization of the TC271 CCD image sensor. Each section briefly describes the measurement and analysis methods that were used and the data and results obtained. The final section summarizes the results of all the measurements in a data sheet format. In most cases, the measurements were performed on a very limited sampling of devices; therefore, lot processing variations should be considered where applicable.

1 Charge Conversion Gain

1.1 Measurement Method and Analysis

The measurement was made using an evaluation PAL-camera board to operate the sensor. An Fe–55 radioactive source from Isotope Product Laboratories with a 5.9-keV photon decay mode was used to provide a known energy source. The photons from the radioactive source produced electrons in the sensor through direct-band transitions in the silicon. These electrons were then shifted to the sensor output amplifier and converted from charge to voltage.

The number of electrons produced per photon event hitting the sensor is given by:

$$N_e = \frac{E_{Fe-55}}{(E_g)_{direct}}$$

where $(E_g)_{direct}$ is the direct-bandgap energy of silicon and $E_{Fe–55}$ is the energy-per-photon event from the radioactive source. At room temperature, the direct bandgap of silicon is 3.64 eV, giving an N_e of 1620 electrons per event. The charge conversion gain is given by:

$$S_o = \frac{V_{out}}{N_e}$$

where V_{out} is the voltage from the pixels where the isotope photon hit.

1.2 Data and Results

The charge conversion gain was measured on five different devices with an average of:

$$S_o = 6.5\,\mu V / e^-$$

2 Dark Current

2.1 Measurement Method and Analysis

The measurement was made using an evaluation PAL-camera board to operate the sensor. The board was placed in a light-tight chamber where the temperature could be varied. The affect of the antiblooming-clock high level on dark current was also measured (the hot-hole induced dark current increases with increasing clock level). The integration time was varied for each case to give a more accurate measurement of the dark current through the slope of the dark voltage versus time curve. The average dark voltage was measured at the sensor output on an oscilloscope and converted to a dark current using:

$$I_d = \frac{dV_d}{d\tau_{int}} \frac{q}{S_o A_p}$$

where S_o is the charge-conversion gain of the CCD readout, A_p is the pixel area, and τ_{int} is the integration time. The temperature dependence of the dark current can be obtained theoretically starting from a rate equation:

$$I_d = q \frac{\kappa_d}{2} N_t \sigma_n v_{th} n_i$$

where q is the magnitude of the electron charge, χ_d is the depletion width, N_t is the trap concentration, σ_n is the electron capture cross section, υ_{th} is the electron thermal velocity, and n_i is the intrinsic carrier concentration. The temperature dependence, T, of the dark current is contained in the thermal velocity:

$$v_{th} = \sqrt{\frac{3kT}{m_n}}$$

where k is Boltzman's constant and m_n is the electron mass; and the intrinsic carrier concentration:

$$n_i = N_C \exp[-(E_C - E_t)/kT]$$

$$with\ N_c = 2\left(\frac{2\pi m_n kT}{h^2}\right)^{3/2}$$

where h is Plank's constant, E_c is the conduction band energy, and E_t is the impurity energy level. To separate the temperature dependence, a temperature independent constant is defined:

$$\gamma_n = \frac{v_{th}}{T^{1/2}} \frac{N_C}{T^{3/2}}$$

$$= 3.25 \cdot 10^{21} \frac{m_n}{m_o}$$

$$= 1.07 \cdot 10^{21}\ cm^{-2} s^{-1} K^{-2}$$

Therefore, the dark current equation can be rewritten:

$$I_d = q\frac{\kappa_d}{2} N_t \sigma_n T^2 \gamma_n \exp(-E_C - E_t)/kT]$$

Dividing by T^2 yields a final equation that can be used to analyze the measured temperature dependent data:

$$\frac{I_d}{T^2} = \frac{q\kappa_d N_t \sigma_n \gamma_n}{2} \cdot \exp\left[\frac{-(E_C - E_t)}{1000k} \cdot \frac{1000}{T}\right]$$

This equation shows that a log-linear plot of I_d/T^2 versus 1000/T (sometimes called an Arrhenius plot) should be linear, and the slope of a linear fit gives the trap activation energy, E_c–E_t:

$$E_c - E_t = -1000 \cdot k \cdot m$$

where m is the slope of the linear fit.

2.2 Data and Results

Figure 1 shows the dark voltage from the CCD as a function of integration time at T = 300 K and VAB_{high} = 4 V. The points are the measured data and the solid line is a linear fit. The variation of dark current over temperature is shown in Figure 2, and the variation with the antiblooming-clock high level is shown in Figure 3. Figure 4 shows the Arrhenius plot with the linear fit to the measured data.

Using a charge conversion tactor of 6.5 µV/e⁻ and a pixel area of 8.4 x 11.4 μm^2 the dark current at T = 300 K and VAB_{high} = 4 V (antiblooming clocking) was found to be:

$$I_d = 100\ pA/cm^2$$

The trap activation energy was found from the Arrhenius plot slope to be:

$$E_C - E_t = 0.58eV$$

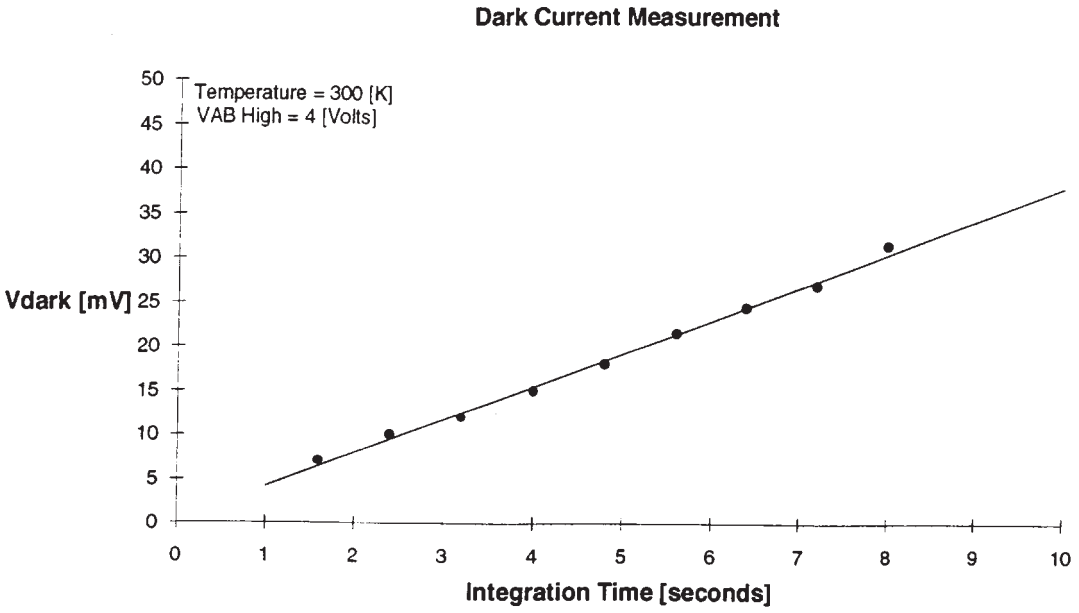

Figure 1. Measured Dark Voltage at the Device Output as a Function of Integration Time Under Normal Operating Conditions

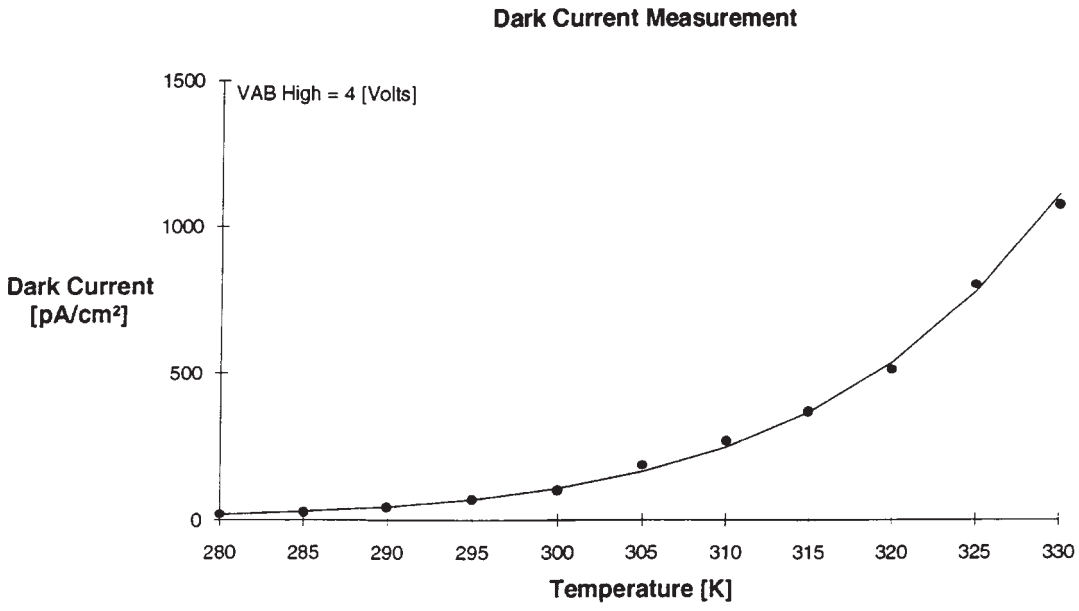

Figure 2. Dark Current as a Function of Temperature

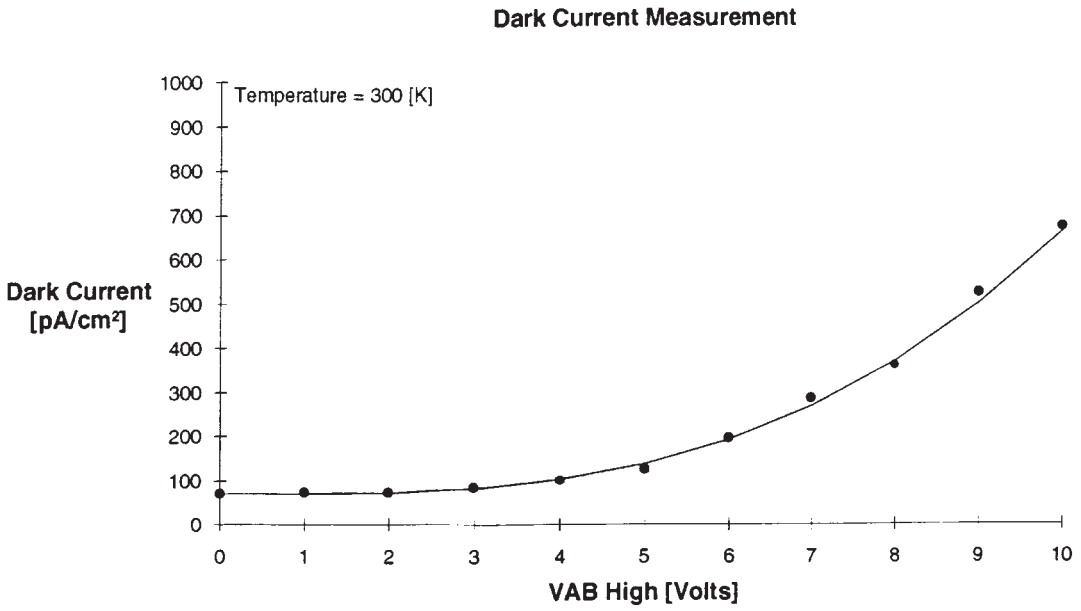

Figure 3. Dark Current as a Function of Antiblooming Clock High Level

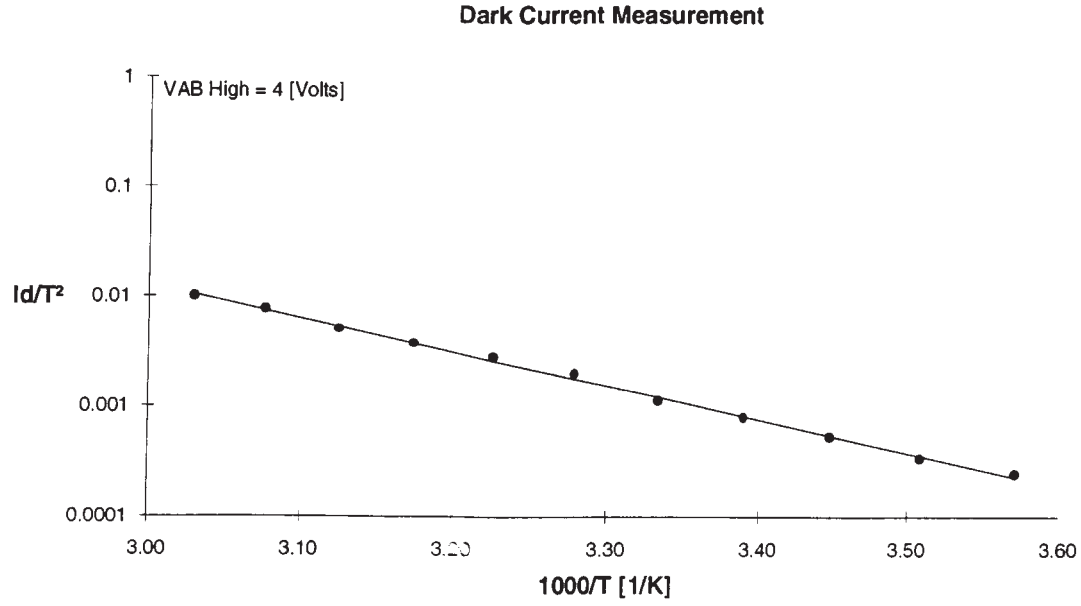

Figure 4. Dark-Current Arrhenius Plot

3 Spectral Characteristics

3.1 Measurement Method and Analysis

The measurement was made using an evaluation PAL-camera board to operate the sensor. A light source was used to supply illumination to the device and optical band-pass filters were used to pass light of restricted wavelength ranges. The entire wavelength range of interest (400 nm to 1000 nm) was spanned by a set of 40-nm wide filters with center wavelengths spaced every 50 nm. The output voltage of the device was measured on the oscilloscope and a light meter was used to measure the irradiant power (units of [Watts/m^2]) of the light incident on the CCD. The responsivity, sensitivity, and quantum efficiency were then calculated from this data. The responsivity was calulated from:

$$\text{Responsivity} = \frac{V_{out}}{P_{light}} \frac{q}{A_p S_o \tau_{int}}$$

where q is the electron charge, A_p is the pixel area, S_o is the charge conversion factor, and τ_{int} is the integration time. The sensitivity was calculated from:

$$\text{Sensitivity} = \frac{V_{out}}{P_{light}} \frac{1}{\tau_{int}}$$

The quantum efficiency was calculated from:

$$\text{Quantum Efficiency} = \frac{V_{out}}{P_{light}} \frac{1}{A_p S_o \tau_{int}} \frac{hc}{\lambda}$$

where h is Plank's constant, c is the speed of light, and λ is the wavelength.

3.2 Data and Results

Figure 5 shows the measurement results. The points are the measured data at the center frequency of the optical band-pass filters and the line is a four-point spline interpolation to the measured data.

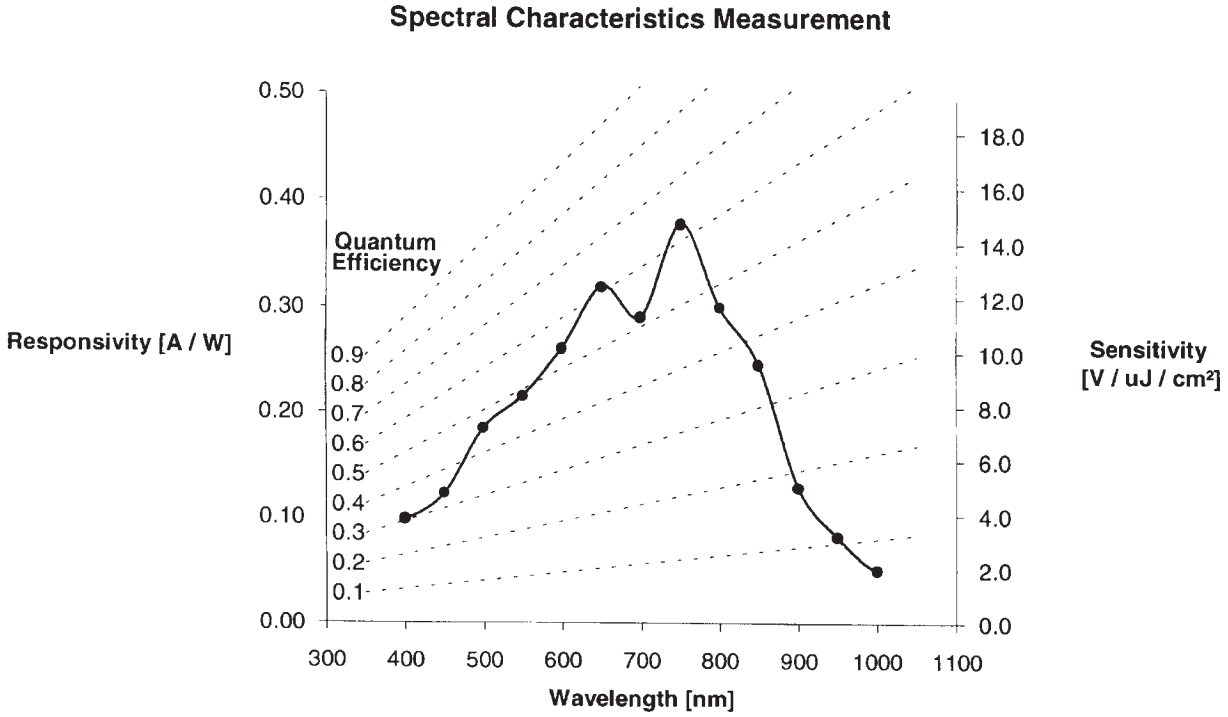

Figure 5. Spectral Characteristics for the Visible and Near IR Wavelengths

4 Light Characteristics

4.1 Measurement Method and Analysis

The measurement was made using an evaluation PAL-camera board to operate the sensor. A light box was used to supply uniform illumination to the device for the sensitivity and saturation-voltage measurements, and a light meter was used to measure the intensity of the illumination in lux. The output voltage of the device was measured on the oscilloscope as the intensity of the illumination was varied.

The sensitivity of the CCD is given by the ratio of the output voltage response (usually in mV) to an input light illumination (usually in lux):

$$S = \frac{V_{out}}{I_{light}}$$

Saturation is defined as the condition where further increase in the illumination does not increase the output voltage. The saturation voltage (V_{sat}) of the device is the output voltage at the saturation condition (with antiblooming off). Using the charge conversion factor, the full-well capacity is obtained from the saturation voltage. The maximum usable signal is defined as the maximum output voltage obtained before antiblooming begins to affect the linear response.

4.2 Data and Results

Figure 6 shows the output voltage of the sensor as a function of light intensity for no antiblooming and with the antiblooming high level at the normal operating voltage.

The following results were obtained from the average of five devices:

- S = 52 mV / lux (with IR filter)
- S = 400 mV / lux (no IR filter)
- Saturation Voltage = 450 mV
- Full Well Capacity = 70,000 electrons
- Maximum Useable Signal = 175 mV

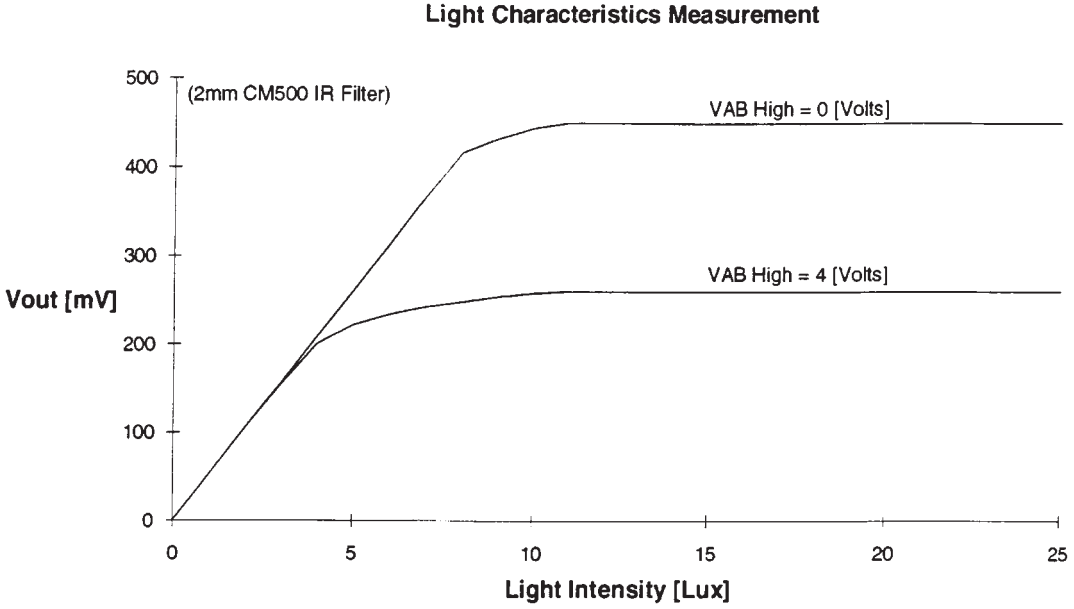

Figure 6. Measured Sensor Output as a Function of Light Intensity

5 Antiblooming Performance

5.1 Measurement Method and Analysis

The measurement was made using an evaluation PAL-camera board to operate the sensor. A laser was used to provide an illumination intense enough to cause blooming while the antiblooming-clock high level was varied. Neutral density filters were used to adjust the laser intensity.

Blooming is defined as the condition where the illumination of a pixel is intense enough that the charge overflows the boundaries of the pixel into another pixel. The blooming-overload ratio is given by the ratio of the light illumination that causes blooming to the light illumination that causes saturation:

$$\text{Blooming Overload Ratio} = \frac{I_{blooming}}{I_{saturation}}$$

5.2 Data and Results

Figure 7 shows the saturation output voltage as a function of the antiblooming-clock high level. Figure 8 shows the blooming overload ratio of the device as a function of the antiblooming-clock high level.

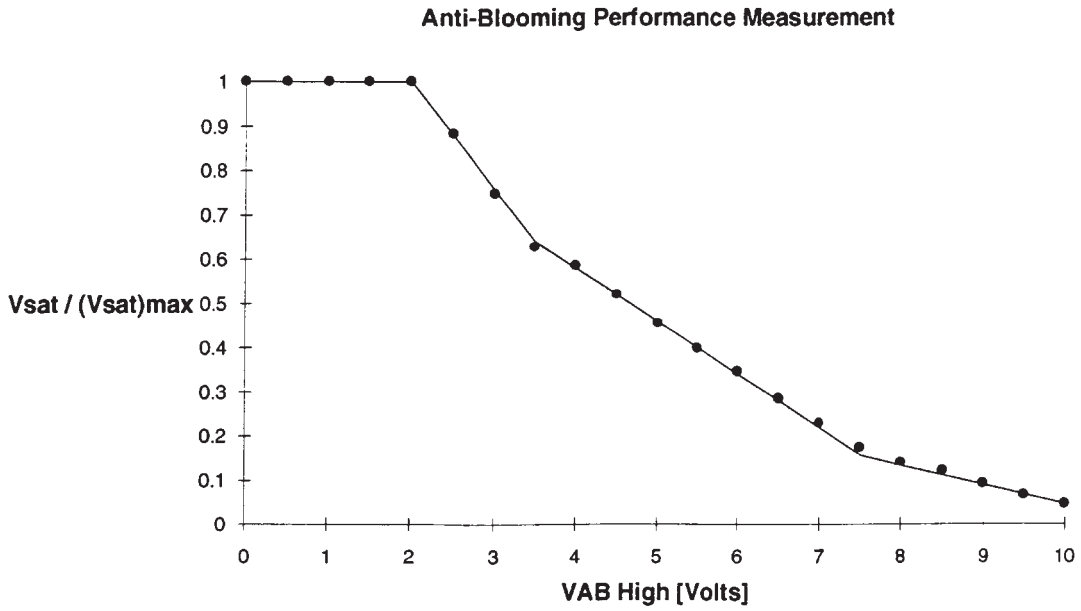

Figure 7. Saturation Voltage as a Function of the Antiblooming High Level

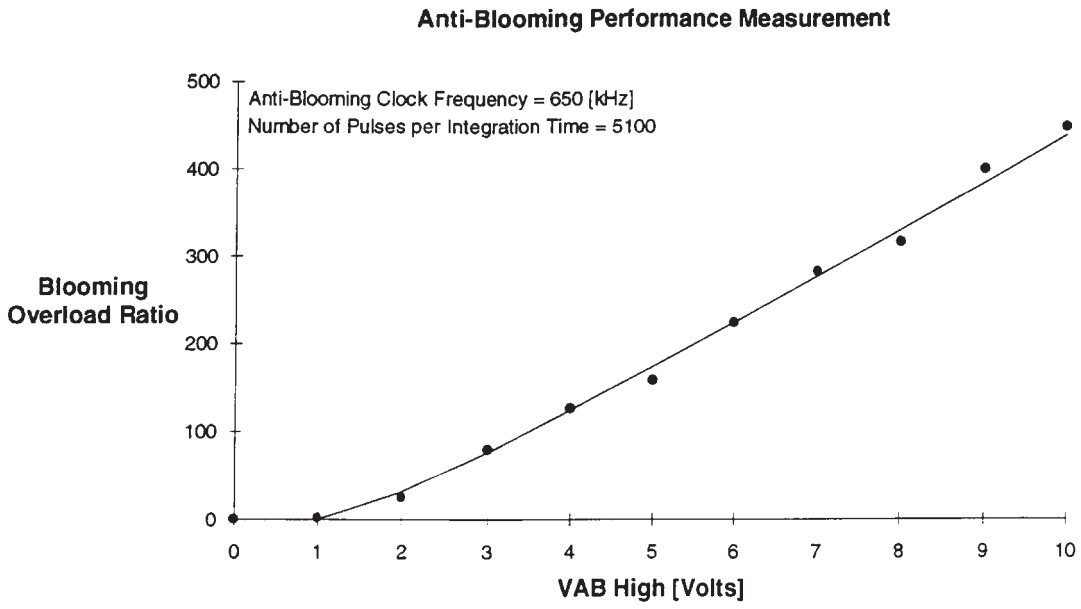

Figure 8. Blooming-Overload Ratio as a Function of the Antiblooming High Level

6 Amplifier Characteristics

6.1 Measurement Method and Analysis

The TC271 amplifier characteristics were measured using a small test board built to operate the on-chip amplifier with a minimum of external disturbances. The following measurements were made:

- Output dc level and amplifier supply current. The output dc level and amplifier current were measured as a function of ADB to determine the operating range for the amplifier.
- Rejection ratios. The rejection ratios of the ADB, SRG, and ABG inputs were measured by inputting an ac signal into the respective input pin and then measuring the resulting signal induced at the device output. The rejection ratio is given by:

$$\text{Rejection Ratio} = 20 \log \frac{V_i}{V_o}$$

  where v_i is the ac signal at the input pin and v_o is the induced signal on the output.

- Output resistance. The output resistance of the on-chip amplifier was measured by varying the load resistance and then measuring the resulting change in the ac output signal magnitude. To calculate the series output resistance, the following formula is used for any two load resistances $R_1{}^L$ and $R_2{}^L$:

$$R_S = \frac{kR_1^L - R_2^L}{1-k} \text{ where } k = \frac{V_1^{out}\, R_2^L}{V_2^{out}\, R_1^L}$$

  where $V_1{}^{out}$ is the ac output signal magnitude for $R_1{}^L$ and $V_2{}^{out}$ is the ac output signal magnitude for $R_2{}^L$.

- Signal-response delay time. The signal-response delay time was measured by comparing the time delay between the ac output signal and the SRG clocks.
- Relative amplifier gain and frequency response. The amplifier gain and frequency response were measured by recording the reset feed through as a function of ADB for the gain and as a function of the SRG frequency for the frequency response.

6.2 Data and Results

Figure 9 shows the output dc level of the amplifier as a function of ADB, and Figure 10 and Figure 11 show the amplifier supply current and power consumption as a function ADB. The amplifier frequency response is shown in Figure 12. Figure 13 shows the amplifier gain as a function of ADB.

The following results were also obtained:

- Output Resistance = 350 Ω
- Signal Response Delay Time = 20 ns
- ADB Rejection Ratio (1 – 50 MHz) = 15 dB
- SRG Rejection Ratio (@ 6.67 MHz) = 45 dB
- ABG Rejection Ratio (@ 6.25 kHz) = 45 dB

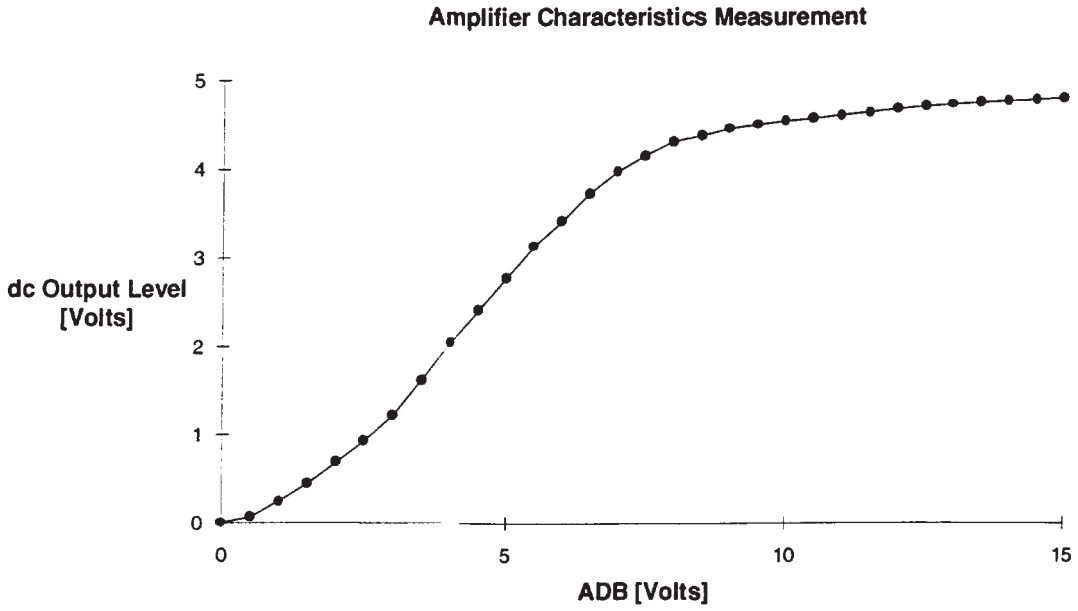

Figure 9. Amplifier Output dc Level as a Function of the Supply Voltage

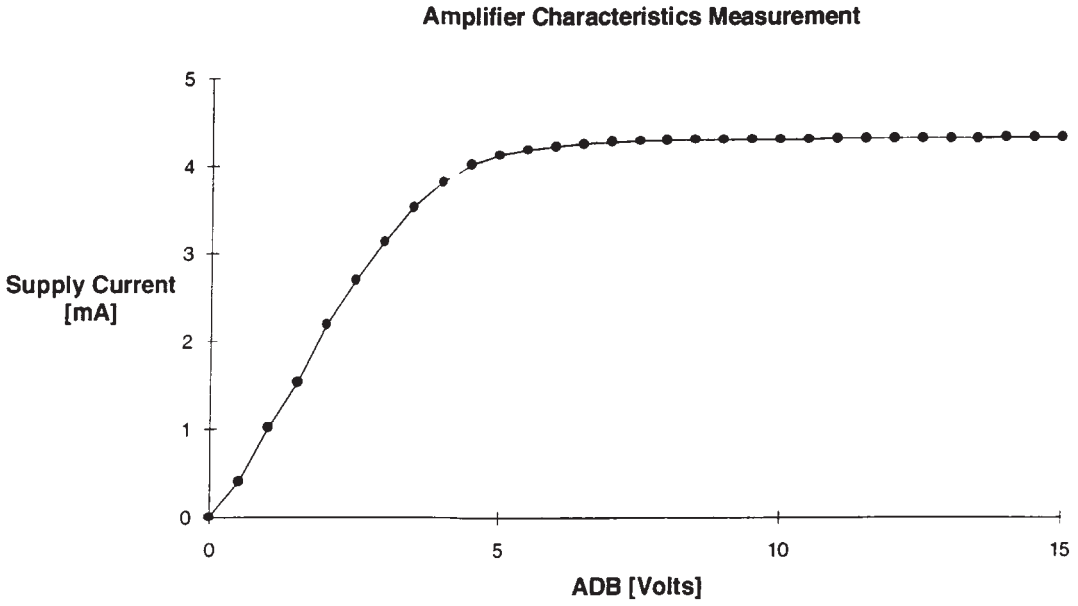

Figure 10. Amplifier Supply Current as a Function of the Supply Voltage

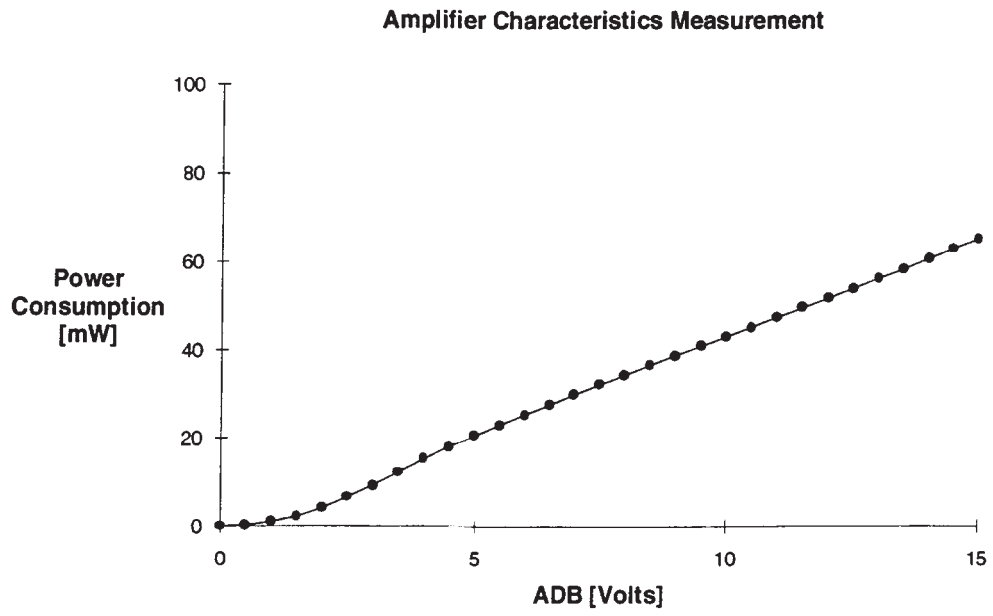

Figure 11. Power Consumption as a Function of the Supply Voltage

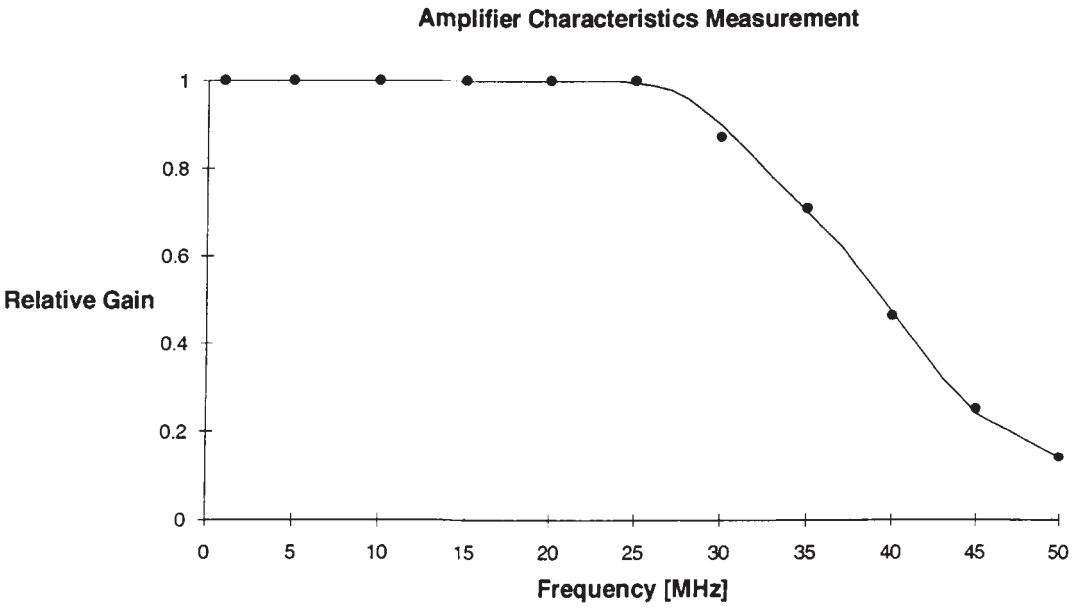

Figure 12. Amplifier Frequency Response Measured Using the Reset Feed Through

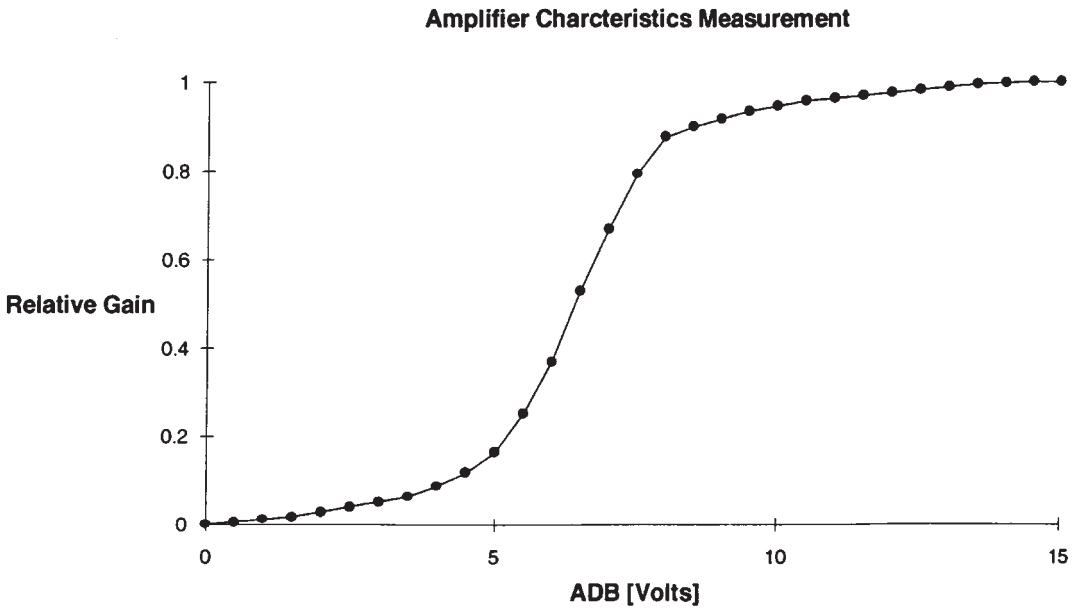

Figure 13. Amplifier Gain Measured Using the Reset Feed Through

7 Gate Characteristics

7.1 Measurement Method and Analysis

The gate-capacitance measurements were made using a Keithley 590 CV analyzer to measure the capacitance versus voltage reponse of the clock gates and the on-chip protection resistors were measured with a dc ohmmeter. The C-V curves of the clock gates are standard MOS-C curves except for the two parallel inversion capacitances due to the different well and barrier regions under one gate. As the gate is swept from accumulation (–10 V) towards inversion (0 V), these different regions cause the C-V curve to reach an equilibrium-inversion capacitance first for the barrier region and then for the well region at a higher voltage.

7.2 Data and Results

The C-V curves measured for the clock gates on the TC271 device are shown in Figure 14. From the C-V curves, the maximum clock capacitances observed during device operation are:

$$(C_{IAG})_{max} = 120000 \text{ pF}$$

$$(C_{SAG1,\ SAG2})_{max} = 110000 \text{ pF}$$

$$(C_{ABG})_{max} = 4600 \text{ pF}$$

$$(C_{TMG})_{max} = 120 \text{ pF}$$

$$(C_{TRG})_{max} = 160 \text{ pF}$$

$$(C_{SRG1,\ SRG2,\ SRG3})_{max} = 80 \text{ pF}$$

The dc load resistances measured for the clocks were:

$$(R_{IAG})_{max} = 53.8 \text{ k}\Omega$$

$$(R_{SAG1,\ SAG2})_{max} = 52.5 \text{ k}\Omega$$

$$(R_{ABG})_{max} = 52.8 \text{ k}\Omega$$

$$(R_{TMG})_{max} = 57.3 \text{ k}\Omega$$

$$(R_{TRG})_{max} = 51.8 \text{ k}\Omega$$

$$(R_{SRG1,\ SRG2,\ SRG3})_{max} = 54 \text{ k}\Omega$$

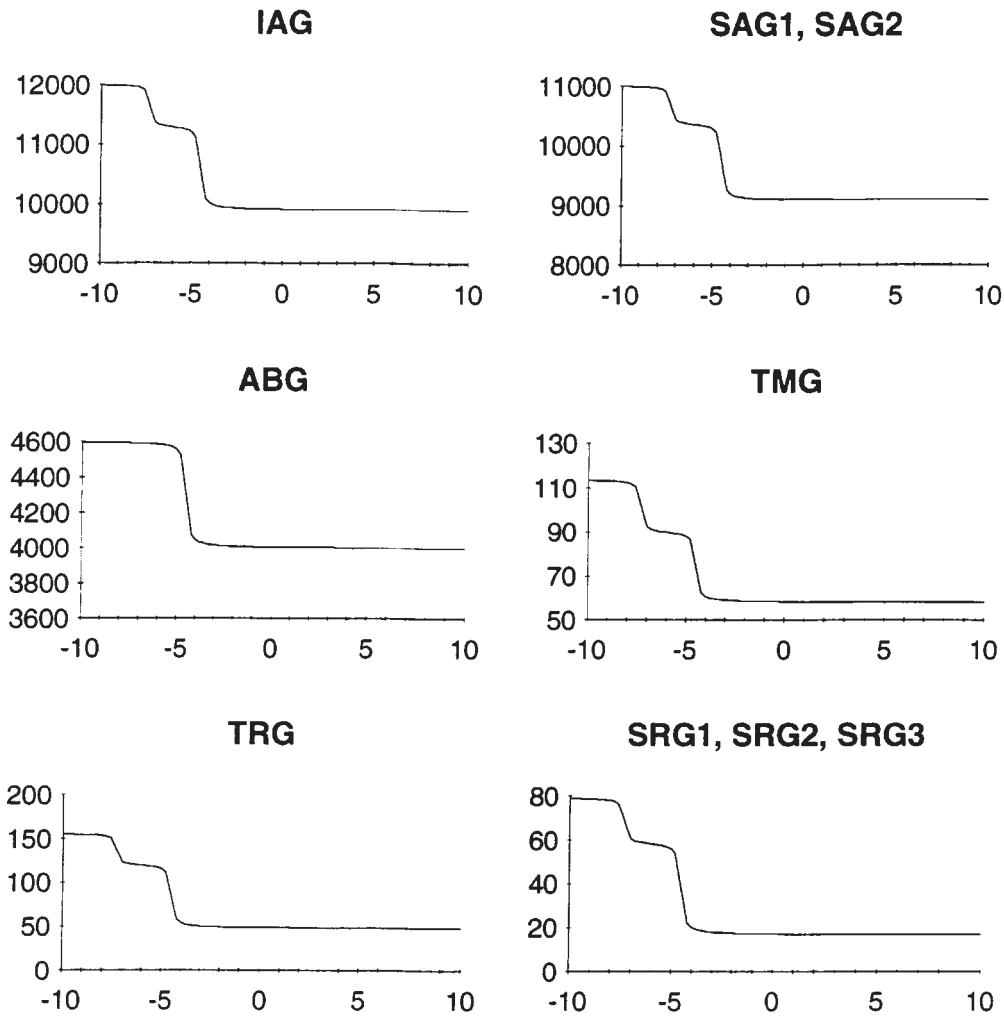

Figure 14. Clock C-V Curves

8 Amplifier Noise

8.1 Measurement Method and Analysis

The TC271 amplifier noise was measured using a small test board built to operate the on-chip amplifier with a minimum of externally generated noise. The amplifier noise was measured using an HP spectrum analyzer. The substrate and clocks on the device were held at ground except for the SRGs that were high, low, or clocking depending on the individual measurement. The reset noise spectrum has been modeled using the following analytical expression:

$$V_{reset}^2(f) = \alpha A_o^2 \cdot V_{kTC}^2 S(2\pi f)$$

Where A_o is the gain of the on-chip amplifier, the factor α is the noise partition constant ($1<\alpha<2$), and the rest is simply the kTC noise from the reset times the noise power spectral density of the reset operation. The output referred kTC noise is given by:

$$V_{kTC}^2 A_o^2 = \frac{kT}{C} A_o^2 = \frac{kT}{q} S_o A_o$$

$$\text{Since } S_o = \frac{q}{C} A_o$$

where k is the Boltzman constant, T is the temperature, q is the electron charge, C is the capacitance of the floating diffusion. and S_o is the amplifier-charge conversion factor. The frequency dependence of the reset noise spectrum is given by:

$$S(\omega = 2\pi f) = \frac{4\omega_f}{\omega_f^2 + \omega^2}(1 + 2\xi \operatorname{sinc}(\omega\delta) - \xi) + 2\tau\xi^2 \operatorname{sinc}^2\left(\frac{\omega\delta}{2}\right)$$

where τ is the period of the reset operation, δ is the width of the reset pulse, $\xi = \delta/\tau$ is the duty cycle of the reset operation, and $\omega f = 1/RC$ is the response frequency of the reset circuit determined by the switch resistance and the capacitance of the floating diffusion. In addition to the reset noise, the output noise of the device includes the broadband white noise of the amplifier that is given by:

$$V_{white}^2 = V_g^{-2} A_o^2$$

where V_g is the input referred value or the white-noise generator in the amplifier. The output noise spectrum is given by:

$$V_n^2(f) = V_{white}^2 + V_{reset}^2$$

$$= V_g^2 A_o^2 + \alpha V_{kTC}^2 A_o^2 S(2\pi f)$$

Setting $f = 0$ in this equation and then solving for ω_f:

$$\omega_f = \frac{\alpha 4 V_{kTC}^2 A_o^2 (1 + \xi)}{V_n^2(0) - V_g^2 A_o^2 - \alpha 2 V_{kTC}^2 A_o^2 \xi^2 \tau}$$

This equation can be used with a measured value of $V_n(0)$ at a reset period τ to calculate the response frequency. Also, setting $f = 0$ and taking the derivative, and then solving for α gives:

$$\alpha = \frac{dV_n^2(f = 0)/d\tau}{2V_{kTC}^2 A_o^2 \xi^2}$$

This equation can be used to calculate the noise partition constant from the slope of a plot of the $V_n(0)$ versus the reset period τ.

The dynamic range of the amplifier is given by:

$$\text{Dynamic Range} = 20 \log \frac{V_{sat}}{V_{rms}}$$

where V_{sat} is the saturation voltage and V_{rms} is the broadband rms value of the amplifier noise.

8.2 Data and Results

Figure 15 shows the squared noise-power spectral density measurement that was used to determine α. Figure 16 shows the noise-power spectral density for the amplifier clocking at normal speed, and Figure 17 shows the dc amplifier measurement with the reset switch on continuously. Figure 18 shows the measured noise-power spectral density with the theoretical model shown. Figure 19 shows the measured noise-power spectral density at f=1 MHz as a function of ADB.

The following results were used in subsequent calculations:

$\tau = 150$ ns
$\xi = 0.5$
$\delta = 75$ ns
$A_o = 0.8$
$S_o = 6.5\ \mu V/e^-$ (from previous measurements)

The output referred kTC noise was calculated to be:

$$V_{kTC}\ A_o = 360\ \mu V$$

The linear fit in Figure 15 gives the noise partition constant to be:

$$\alpha = 1.25$$

The broadband white noise of the amplifier was obtained from Figure 17 to be:

$$V_g\ A_o = 25\ nV/\sqrt{HZ}$$

Using $V_n(0) = 150\ nV/\sqrt{HZ}$ at $\tau = 150$ ns from gave the response frequency to be:

$$\omega_f = 100\ Mrad/s$$

The above values produced the theoretical curve shown in Figure 18 for the power spectral density. Integrating this from 15.7 kHz (line clamp rate) to 60 MHz (amplifier bandwidth) gave the RMS noise to be:

$$(V_n)_{RMS} = 400\ \mu V = 62\ \text{electrons}$$

The dynamic range of the device was calculated using a saturation voltage of 450 mV:

$$\text{Dynamic Range} = 61\ dB$$

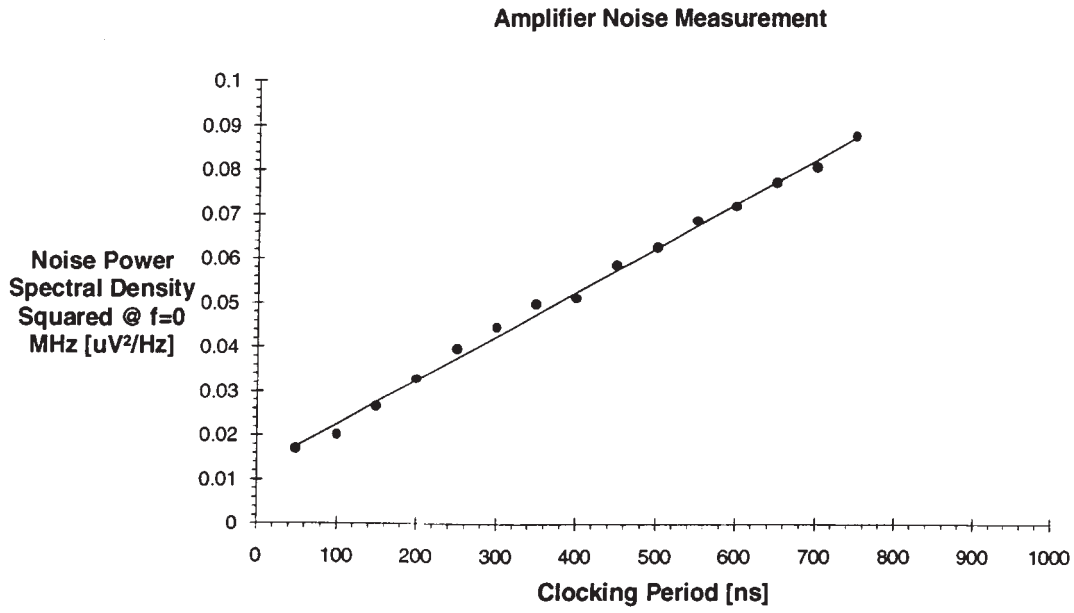

Figure 15. Squared Noise-Power Spectral Density Measured at f = 0 as a Function of the Reset Period

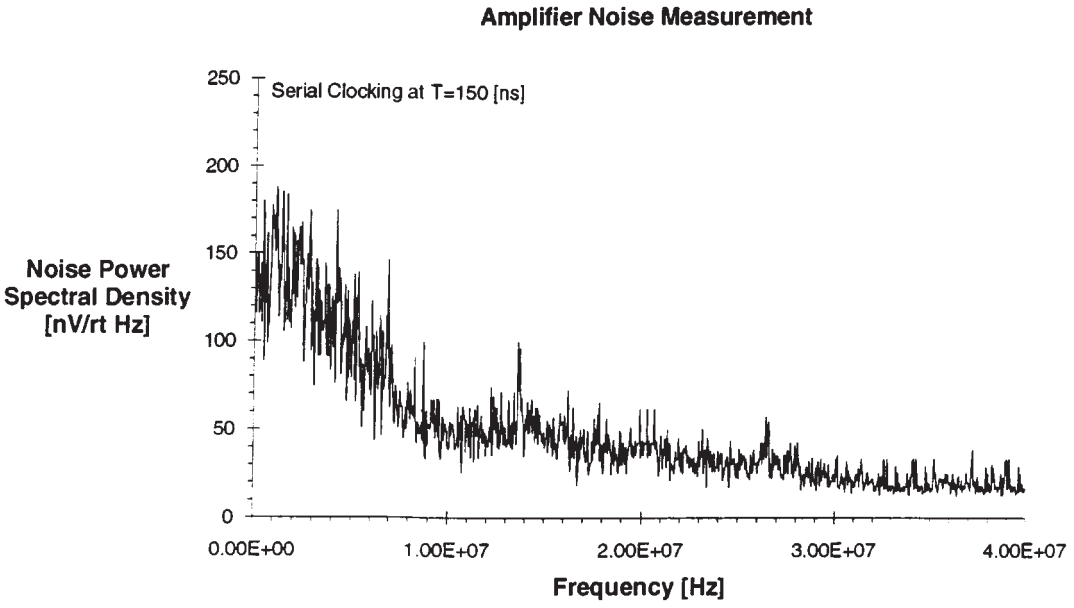

Figure 16. Noise-Power Spectral Density Measured at the Normal Serial-Clocking Speed

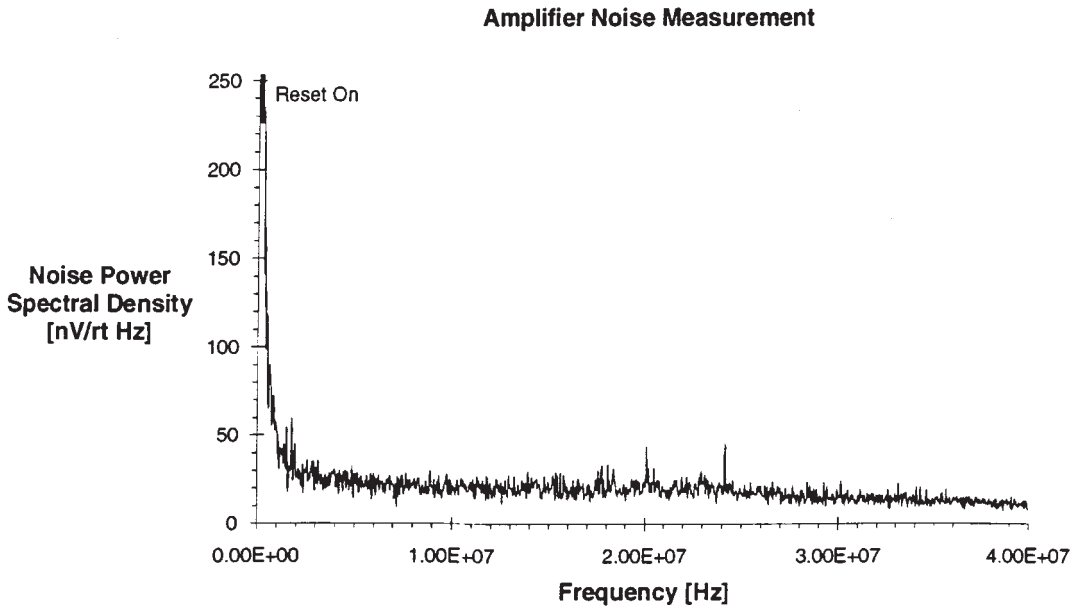

Figure 17. Noise-Power Spectral Density Measured With Reset On

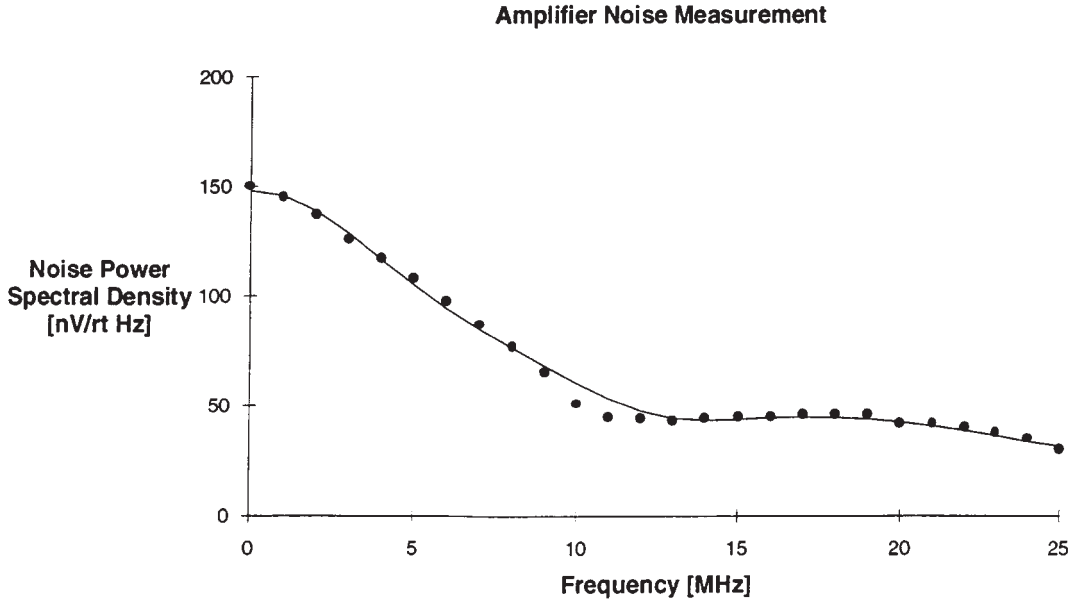

Figure 18. Noise-Power Spectral Density, Measured for τ = 150 ns, With the Solid Line for the Theory

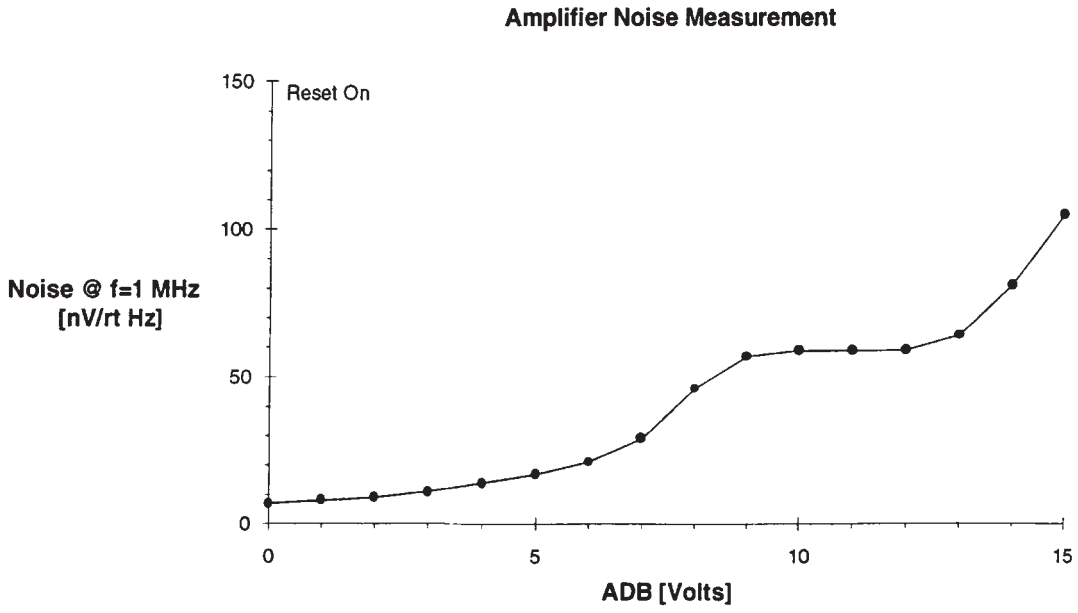

Figure 19. Noise-Power Spectral Density Measured at f = 1 MHz with Reset On, as a Function of the Amplifier Supply Voltage

9 Data Summary

9.1 Operating Conditions

PARAMETER			MIN	NOM	MAX	UNIT
ADNB			10	11	12	V
SUB				0		V
Clock level	IAG	High	1	2	3	V
		Low	−9	−8	−7	
	SAG1, SAG2	High	1	2	3	
		Low	−9	−8	−7	
	ABG	High	2/5	4	5	
		Intermediate		−2.5		
		Low	−8	−7	−6	
	TMG	High	1	2	3	
		Low	−9	−8	−7	
	TRG	High	1	2	3	
		Low	−9	−8	−7	
	SRG1, SRG2, SRG3	High	1	2	3	
		Low	−9	−8	−7	
Clock frequency	IAG			1.11		MHz
	SAG1, SAG2			6.67		
	ABG			0.625		
	TMG			6.67		
	TRG			1.67		
	SRG1, SRG2, SRG3			6.67		
Clock transition	IAG			40		ns
	SAG1, SAG2			40		
	ABG			40		
	TMG		50	50		
	TRG			10		
	SRG1, SRG2, SRG3			40		
Capacitive load				7		pF

9.2 Electrical Characteristics

PARAMETER		MIN	NOM	MAX	UNIT
Dynamic range			60		dB
Charge-conversion factor			6.5		μV/e⁻
Charge-transfer efficiency			0.999		
Signal-response delay time			20		ns
Power consumption			50		mW
Amplifier supply current			4.5		mA
Output resistance			350		Ω
Output dc level			4.5		V
Noise spectrum			see Figure 16		μV/rt Hz
Noise equivalent signal			60		electrons
Rejection ratio	(1–50 MHz) ADB		15		dB
	(@ 6.67 MHz) SRG		45		
	(@ 625 kHz) ABG		45		
Clock capacitance	IAG		12000		pF
	SAG1, SAG2		11000		
	ABG		4600		
	TMG		120		
	TRG		160		
	SRG1, SRG2, SRG3		80		
Clock load resistance	IAG		54		kΩ
	SAG1, SAG2		53		
	ABG		53		
	TMG		57		
	TRG		52		
	SRG1, SRG2, SRG3		54		

9.3 Optical Characteristics

PARAMETER	MIN	NOM	MAX	UNIT
Pixel size		96		μm^2
Sensitivity with CM500 (2 mm)		52		mV/lux
Sensitivity without IR filter		400		mV/lux
Spectral characteristics		see Figure 5		
Saturation voltage		450		mV
Maximum useable signal		175		mV
Blooming overload ratio		125		
Dark current		100		pA/cm^2
Dark signal		150		μV
Full-well capacity		70000		electrons

REFERENCES

John C. Feltz, “Development of the Modulation Transfer Function and Contrast Transfer Function for Discrete Systems, Particularly Charge-Coupled Devices”, *Optical Engineering*, 893-904 (August 1990).

Harold Hosack, “Aperture Response and Optical Performance of Patterned-Electrode Virtual-Phase Imagers”, *IEEE Transations On Electron Devices*, Vol. ED-28, No. 1, January 1981.

M. J. Howes and D. V. Morgan, Charge-Coupled Devices and Systems, *Wiley Series in Solid State Devices and Circuits*, 1979.

S. M. Hsieh and H. H. Hosack, “Low Light Level Imaging with Commercial Charge-Coupled Devices”, *Optical Engineering* 26(9), 884-889 (September 1987).

Jaroslav Hynecek, “Virtual Phase Technology: A New Approach to Fabrication of Large-Area CCDs”, *IEEE Transactions on Electron Devices*, Vol. Ed-28, No. 5, May 1981.

Jaroslav Hynecek, “Electron-Hole Recombination Antiblooming For Virtual Phase CCD Imager”, *IEEE Transactions on Electron Devices*, Vol. ED-30, No. 8, August 1983.

Jaroslav Hynecek, “Design And Performance Of A Low-Noise Charge Detection Amplifier For VPCCD Devices”, *IEEE Transactions on Electron Devices*, Vol. ED-31, No. 12, December 1984.

Jaroslav Hynecek, “Design and Performance of a High-Resolution Image Sensor for Color TV Applications”, *IEEE Transactions on Electron Devices*, Vol. ED-32. No. 8, August 1985.

Jaroslav Hynecek, “High-Resolution 8-mm CCD Image Sensor with Correlated Clamp Sample and Hold Charge Detection Circuit”, *IEEE Transactions on Electron Devices*, Vol. ED-33, No. 6, June 1986.

Jaroslav Hynecek, “A New High-Resolution 11-mm Diagonal Image Sensor for Still-Picture Photography”, *IEEE Transactions on Electron Devices*, Vol. 36, No. 11, November 1989.

Jaroslav Hynecek, “Spectral Analysis of Reset Noise Observed in CCD Charge-Detection Circuits”, *IEEE Transactions On Electron Devices*, Vol. 37, No. 3, March 1990.

Jaroslav Hynecek, “BCMD – An Improved Photosite Structure for High Desnsity Image Sensors”, *IEEE Transactions on Electron Devices*, Vol. 38, No. 5, May 1991.

Paul G. Jesper, Fernand Van de Viele, and Marvin H. White editors, SOLID STATE IMAGING – Proceedings of the NATO Advanced Study Institute on Solid State Imaging, held in Louvain-la Neuve, Belgium, September 3-12, 1975, 1976, Noordhoff International Publishing.